

# Data-Driven Approaches for Measurement Interpretation: Analysing Integrated Thermal and Vehicular Response in Bridge Structural Health Monitoring

*Rolands Kromanis\*<sup>a</sup> and Prakash Kripakaran<sup>b</sup>*

*<sup>a</sup> Civil Engineering Department, Nottingham Trent University, UK; <sup>b</sup> College of Engineering, Mathematics and Physical Sciences, University of Exeter, UK.*

**Abstract:** A comprehensive evaluation of a structure's performance based on quasi-static measurements requires consideration of the response due to all applied loads. For the majority of short- and medium-span bridges, temperature and vehicular loads are the main drivers of structural deformations. This paper therefore evaluates the following two hypotheses: (i) knowledge of loads and their positions, and temperature distributions can be used to accurately predict structural response, and (ii) the difference between predicted and measured response at various sensor locations can form the basis of anomaly detection techniques. It introduces a measurement interpretation approach that merges the regression-based thermal response prediction methodology that was proposed previously by the authors with a novel methodology for predicting traffic-induced response. The approach first removes both environmentally (temperature) and operationally (traffic) induced trends from measurement time series of structural response. The resulting time series is then analysed using anomaly detection techniques. Experimental data collected from a laboratory truss is used for the evaluation of this approach. Results show that (i) traffic-induced response is recognized once thermal effects are removed, and (ii) information of the location and weight of a vehicle can be used to generate regression models that predict traffic-induced response. As a whole, the approach is shown to be capable of detecting damage by analysing measurements that include both vehicular and thermal response.

**Keywords:** structural health monitoring, long-term bridge monitoring, thermal response, temperature effects, signal processing, anomaly detection

## Abbreviations

TIC – thermal imaging camera;  
RBTRP – regression-based thermal response prediction;  
TIRP – traffic-induced response prediction;  
PE – prediction error;  
PCA – principal component analysis;  
SVR – support vector regression;  
SSM – signal subtraction method.

## 1. Introduction

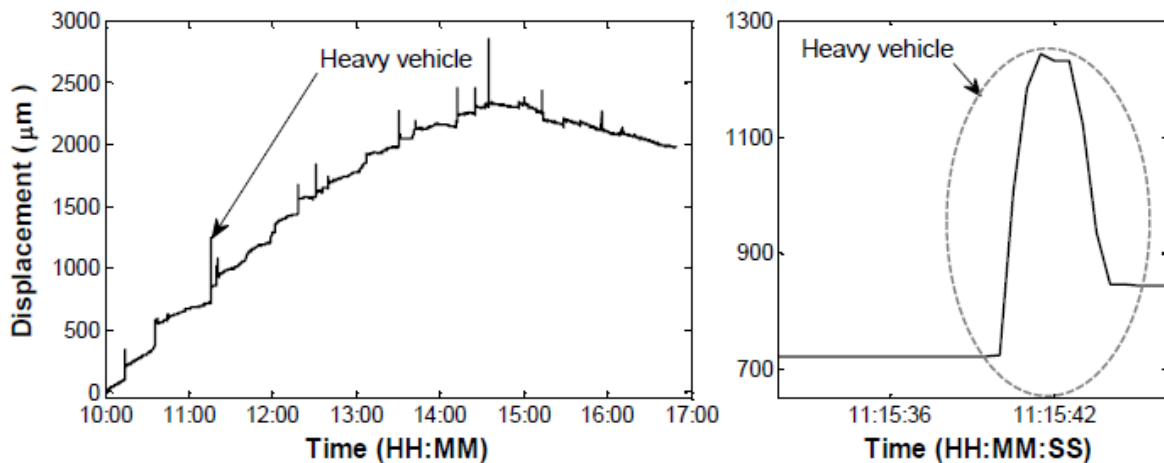
Bridges are important transportation links, and their uninterrupted operation is vital for a functioning economy and society. Current procedures for their structural management are based largely on visual inspections that can be unreliable and highly subjective [1,2]. Furthermore, since detailed visual inspections are expensive requiring significant engineer time, they are performed sporadically. For example, in the UK, principal inspections that require engineers to examine each bridge component by getting within touching distance are

41 typically performed only once every 6 years [3]. Consequently, concerns affecting bridge  
42 performance are often identified at an advanced stage, thereby requiring expensive structural  
43 interventions that are disruptive to the operation of transport networks. Such reactive  
44 approaches to bridge management also leads to huge maintenance backlogs that greatly  
45 undermines the capacity of the transport infrastructure. In the UK, the maintenance backlog for  
46 works on the 57,000 bridges, which are owned and operated by the local highway authorities  
47 and estimated to be worth £24 billion, was over £2.4 billion or about 10% of their value as per  
48 2007 estimates [4]. In the USA, according to data submitted to Federal Highways  
49 Administration in 2015, 58,791 bridges (9.6% of the bridge stock) were classified as  
50 structurally deficient [5] and the total costs of their rehabilitation were predicted to be \$31  
51 billion. There is therefore great interest among the bridge engineering community in deploying  
52 sensing technologies, which can provide reliable, continuous data streams about bridge loading  
53 and response, as a useful complement to visual inspections [6–9].

54 The main challenge in sensing-based bridge management is in relating collected measurements  
55 to structural performance. Response time histories can be complex to analyse for a variety of  
56 reasons. They contain a certain degree of noise due to sensor characteristics. Outliers arising  
57 from occasional sensor malfunction or data acquisition issues are also often present. However,  
58 more important is the fact that the structural response and hence the measurements are strongly  
59 affected by the various loads on the structure including environmental factors and vehicular  
60 traffic. Previous research has shown that environmental loads, which vary both diurnally and  
61 seasonally, leave a strong signature in the response time histories [10]. Specifically,  
62 temperature effects on bridge response can exceed those of other environmental and  
63 operational loads [11]. Traffic induced-response appear as short spikes superimposed on  
64 thermal response [12]. For example, Figure 1 (left) shows time histories of the horizontal  
65 movement measured at the expansion joint of the River Exe Bridge. Spikes in the horizontal  
66 movement are induced by heavy vehicles crossing the bridge. Figure 1 (right) is a zoomed-in  
67 view of a portion of the displacement time-history that corresponds to the passage of a heavy  
68 truck over the bridge. Consequently, simple approaches for detecting damage that ignore how  
69 the response is affected by the various loads are not useful for real-life structures. For example,  
70 the concept of detecting damage by using threshold bounds on individual measurements  
71 seldom works since the effect of damage on structural response is often much smaller than the  
72 change in response due to diurnal and seasonal temperature variations [13].

73 Data-driven techniques that exploit patterns arising from spatial and temporal correlations in  
74 measurements are well-suited to deal with the above-mentioned complexities in measured  
75 response time histories. Since these techniques do not rely on a physics-based model of the  
76 structure, they can be more effective than model-based methods for dealing with the potentially  
77 large volumes of measured data. Data-driven techniques usually require a training data-set  
78 comprising measurements representing baseline conditions of a bridge. The techniques extract  
79 features representative of normal structural behaviour from the training data-set and then  
80 compare these features with those extracted from new measurements to detect changes in  
81 structural behaviour [14].

82 Data-driven techniques are adapted typically from quantitative fields such as econometrics [15]  
 83 and statistics [16]. However, a few techniques such as mathematical correlation models [17]  
 84 and linear approaches to modelling nonlinearities [18] have also been developed specifically  
 85 for interpreting bridge monitoring data. The majority of currently available data-driven  
 86 techniques are concerned with the interpretation of response time histories and are able to  
 87 detect the onset of damage only in simulated measurements created using numerical models of  
 88 bridges that model damage as a reduction in stiffness [16]. They fail to demonstrate similar  
 89 performance for measurements from real-life structures particularly when damage is located  
 90 away from sensors [19] due to the presence of environmental trends that mask damage effects  
 91 on response. Laory et al. [20] hence studied the removal of seasonal variations from  
 92 measurements through use of a moving average filter and a low-pass filter. However, this had  
 93 the negative effect of reducing damage detectability. Laory et al. [21] later combined two data-  
 94 driven methods, specifically moving principal component analysis with robust regression  
 95 analysis, to enhance damage detectability. However, the performance of the resulting approach  
 96 has been illustrated only on measurements collected during the construction phase of a bridge.



97  
 98 Figure 1 The River Exe Bridge: time histories of the horizontal movement of the steel  
 99 girder at the expansion joint collected over 7 hours (left) and during the passage of a heavy  
 100 vehicle (right). (Courtesy: Dr David Hester and Devon County Council.)

101 Kromanis and Kripakaran [22] suggested a novel data-driven methodology referred to as  
 102 Regression-Based Thermal Response Prediction (RBTRP) methodology for predicting thermal  
 103 response, which is the main constituent of the environmental trend in measured response time  
 104 histories. They demonstrated that measurements of temperature distributions can be exploited  
 105 to predict accurately thermal effects in measured response. They also showed that the time  
 106 histories resulting from subtracting the predicted thermal response from the measured response  
 107 time histories can be analysed by anomaly detection techniques for damage detection. Other  
 108 researchers have also since investigated similar methods that use both temperature and  
 109 deformation measurements for damage detection. Yarnold et al [23] showed that distributed  
 110 temperature and deformation measurements can enable damage detection albeit through the  
 111 use of physics-based (finite element) models. This research aims to combine the authors'  
 112 previous work in predicting thermal response with a novel methodology for predicting  
 113 vehicular response in order to create a damage detection approach that is capable of analysing

114 response time histories containing both temperature and vehicular effects. There are no data-  
115 driven approaches that currently offer this capability.

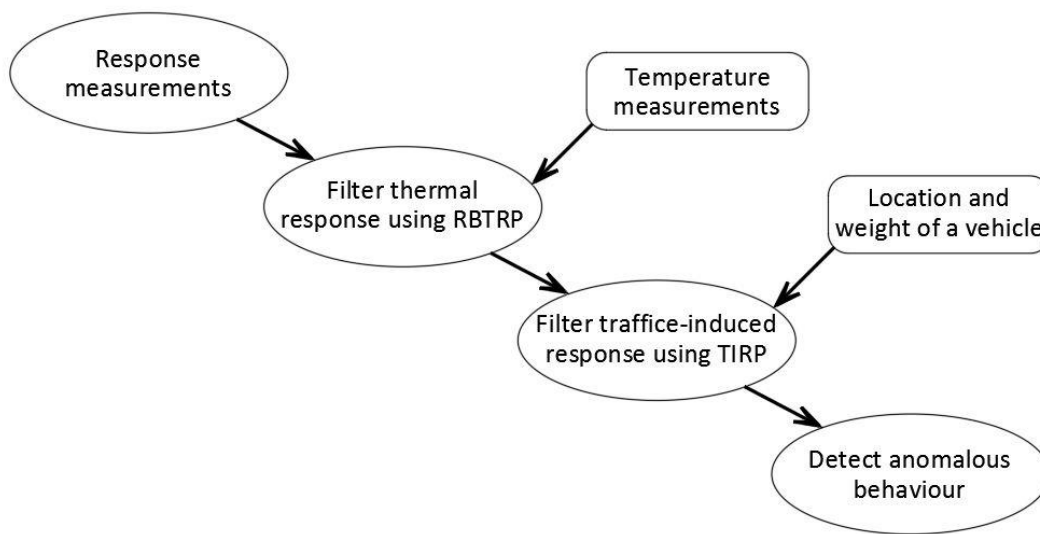
116 This study will rely on knowledge of vehicular loads and their positions on the bridge to predict  
117 vehicular response. Technologies for measuring vehicle load and location are now well-  
118 developed. For example, coupling data from vision-based systems with data from other sensing  
119 devices can enable identification of the location, number and types of vehicles, hence,  
120 supporting the characterization of their induced response. Such concepts have already been  
121 demonstrated in many studies. Glisic et al. [24] have proposed data management principles for  
122 accessing and visualizing measurements collected with contact sensors and video streaming.  
123 The background subtraction method has been shown to be useful to analyse video-streamed  
124 images to identify location, type and speed of a vehicle for anomaly detection [25]. Axle loads  
125 of a vehicle can be determined using weigh-in-motion sensors [26]. Video streams of traffic  
126 from a bridge have also been combined with displacement measurements to create influence  
127 lines, which then serve as input features into anomaly detection methodologies [25]. Therefore,  
128 this paper examines how to utilise the knowledge of vehicular and environmental loads, which  
129 are increasingly available through measurements from continuous monitoring, to better  
130 understand real-time structural performance.

131 This paper will first describe the overall approach for measurement interpretation including  
132 how it will combine methodologies for predicting thermal and vehicular response in a  
133 framework for anomaly (damage) detection. This will be followed by a background on the  
134 RBTRP methodology for predicting thermal response, and then a description of the novel  
135 Traffic-Induced Response Prediction (TIRP) methodology to predict vehicular response. It will  
136 later discuss the anomaly detection techniques used to analyse the time histories produced after  
137 subtracting thermal and vehicular response from the measured response time histories. The  
138 overall approach will be illustrated using measurements collected from a truss that has been  
139 built and continuously monitored in the structures laboratory at the University of Exeter. The  
140 paper will finish with a discussion of the results, conclusions and limitations of the work.

## 141 **2. Measurement interpretation approach**

142 The premise of this study is that information of inputs (loads) into and outputs (response) from  
143 a structural system are available via monitoring. The vision is to develop separate data-driven  
144 methodologies to predict the structural response due to each load and ambient parameter. This  
145 will enable filtering the effects of vehicular and environmental loads from measured response  
146 time histories and then analysing the resulting time histories using anomaly detection methods.  
147 As a first step towards this goal, traffic and temperature effects alone are considered in this  
148 research. All other environmental factors (e.g. wind) are assumed to have no effect on a  
149 bridge's structural response. The overall measurement interpretation approach is schematically  
150 illustrated in Figure 2. Predictions from two methodologies: (1) the RBTRP methodology and  
151 (2) TIRP methodology are used to filter thermal and vehicular response respectively from  
152 measured response. Both the methodologies for predicting structural response, in order to be  
153 useful for real-time measurement interpretation, have to be computationally inexpensive and

154 potentially applicable to a range of structures. Regression-based models that capture the  
 155 relationship between structural deformations (e.g. strain, displacement) and loadings (e.g.  
 156 temperature, traffic) and their locations are well-suited for this task [22], and therefore form  
 157 the basis of the RBTRP and TIRP methodologies. The time histories resulting from subtracting  
 158 the predicted thermal and vehicular response from measured response time histories are  
 159 effectively response-free signals. Response-free signals would be zero signals if the traffic- and  
 160 temperature-induced response are predicted perfectly by the corresponding methodologies, and  
 161 if the measurements were free of noise and outliers. These response-free signals are  
 162 subsequently analysed for anomalies using signal processing techniques. All the elements of  
 163 the overall approach starting with the RBTRP methodology are described in the following  
 164 subsections.



165

166 Figure 2 A schematic of the proposed measurement interpretation approach.

167 **2.1. Regression-based thermal response prediction (RBTRP) methodology**

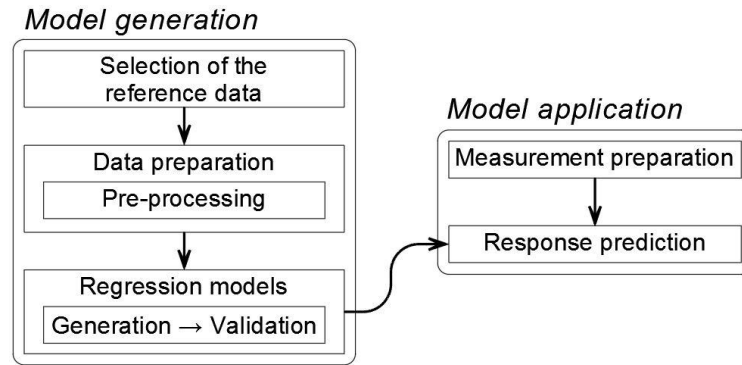
168 The RBTRP methodology is built on a premise that the thermal response of a bridge can be  
 169 determined from knowledge of its current temperature distributions and an understanding of  
 170 the relationship between temperature distributions and structural response obtained from a set  
 171 of reference measurements. The RBTRP methodology consists of the following two phases as  
 172 shown in Figure 3.

- 173 1) Model generation phase: This phase generates regression models that use information  
 174 of temperature distributions as input to predict thermal response. It involves a series of  
 175 iterations over the following interlinked steps:
- 176 a. *Reference set selection*: First a reference period is chosen during which the  
 177 structure is considered to be behaving normally. Measurements collected during  
 178 this period but without traffic on the bridge are split into training and test sets  
 179 for the purpose of training regression models and evaluating their performance  
 180 respectively.

181           b. *Data preparation*: Measurements are treated for outliers using the interquartile  
182 range technique, which has been shown to effectively remove outliers in  
183 previous studies [16]. The moving averaging filter is then employed to smooth  
184 the measurements to minimize effects of noise. If required, measurements are  
185 then down-sampled to an appropriate frequency in order to ensure model  
186 training is not too computationally demanding due to the size of the data set.  
187 Lastly the dimensionality of the data set of temperature measurements, which  
188 will constitute the input to the regression models, is reduced using principal  
189 component analysis (PCA), which takes advantage of inherent correlations  
190 between variables in the data-set [27]. PCA finds a set of principal component  
191 vectors defining an orthogonal transformation from the original set of variables  
192 which are linearly-correlated to a new set of variables which are uncorrelated.  
193 According to [28], the first one-third of the principal components covers  
194 99.99% of the variability in temperatures. Hence these principal components  
195 alone are sufficient as input to the regression models. This step also accounts  
196 for thermal inertia effects in the measured data. Thermal inertia refers to the  
197 phenomenon of internal material temperatures lagging significantly behind  
198 ambient temperatures. Consequently the time series of response and  
199 temperature measurements may appear to be out of phase. This is particularly  
200 the case in concrete structures due to their voluminous nature, high thermal mass  
201 and low thermal conductivity. Thermal inertia effects are effectively  
202 incorporated within the regression models by providing the principal  
203 components corresponding to temperatures measured at both the current time-  
204 step and a previous time-step as input [22,29].

205           c. *Training and evaluation of regression models*: In this step, regression models  
206 are trained using the training data sets. The performance of the trained models  
207 is evaluated subsequently on test data sets. The above-mentioned steps are  
208 performed iteratively for various kinds of regression models such as support  
209 vector regression (SVR) and multiple linear regression. For any chosen  
210 regression algorithm, the models are generated iteratively by varying parameter  
211 settings until improvements in prediction accuracy are observed to be  
212 negligible. However since results from previous studies [22] on thermal  
213 response prediction that have compared various types of regression models  
214 support the effectiveness of SVR for this task, results using SVR models alone  
215 are shown in this paper.

216       2) Model application phase: In this phase, regression models offering the highest  
217 prediction accuracy are employed to predict real-time thermal response from measured  
218 temperature distributions. First temperature measurements are prepared for input to the  
219 chosen regression model. Measurements are treated for outliers and smoothed, and their  
220 dimensionality is reduced using PCA. The first few principal components are provided  
221 as input to the regression models to predict thermal response.



222

223 Figure 3 Flowchart showing the strategy for response prediction methodology.

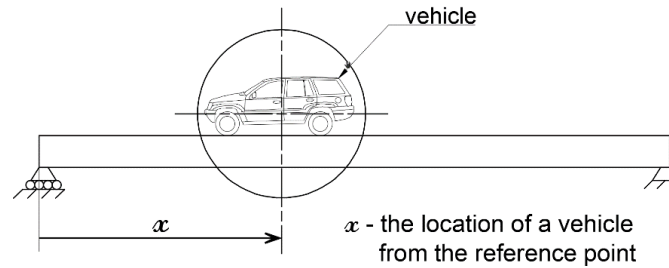
224 **2.2. Traffic-induced response prediction (TIRP) methodology**

225 The TIRP methodology is built on a premise that the traffic-induced response of a bridge can  
 226 be determined from knowledge of the traffic loads and their locations, and an understanding of  
 227 the relationship between traffic load parameters and structural response obtained from a set of  
 228 reference measurements. Theoretically, a single crossing of a vehicle and the respective  
 229 measured deformations can provide sufficient information to determine relationships between  
 230 load, its location and response. These relationships can form the basis of regression models that  
 231 predict displacements induced by similar type of vehicles at any location along the length of  
 232 the structure. In real-life, however, displacements may not always resemble previously  
 233 measured values even under the same traffic load. For example, bearings may lock temporarily,  
 234 creating restraints that change structural behaviour. For these reasons, a broad set of traffic and  
 235 response data is needed to generate robust and accurate prediction models. Furthermore,  
 236 temperature effects may persist in the response measurements even after subtracting predicted  
 237 thermal response using RBTRP methodology as will be shown later in the paper using the case  
 238 study. This is expected as material properties and hence the structure's stiffness can vary with  
 239 changes in temperature distributions. For this reason, in addition to information of the  
 240 magnitude of the applied load and its location, the first few PCs of temperatures are also  
 241 provided as input variables for the TIRP methodology.

242 The TIRP methodology follows a process similar to that of the RBTRP methodology (Figure  
 243 3) for training and applying regression-based models. Figure 4 illustrates the concept employed  
 244 to identify the location of a vehicle on a bridge. For the purpose of simplicity, the bridge is  
 245 assumed to have a single lane and only one vehicle is assumed to be on the bridge at any time.  
 246 The length of the bridge is split into 100 segments. The segments are numbered sequentially  
 247 from the left support. The location of a vehicle is defined by the number of the segment in  
 248 which the centre of the vehicle is located.

249 In the model generation phase, as for the RBTRP methodology, data set from a reference period  
 250 is chosen for training purposes. This data set, which includes measurements of temperature  
 251 distributions and response as well as vehicle loads and locations, is first pre-processed. After  
 252 removing outliers and noise, thermal response, as predicted by the RBTRP methodology using  
 253 the temperature measurements, is subtracted from the response measurements to identify the  
 254 response due to only traffic loads. Using this response data, regression models are trained to

255 predict the traffic-induced response using the locations and the weights of the vehicles, and the  
 256 first few principal components of temperature measurements as input. The best models for  
 257 traffic response prediction are then selected. These models are used in the model application  
 258 phase (Figure 3) to predict the traffic-induced response in real-time based on measured  
 259 temperatures and vehicle loads and their locations.



260

261 Figure 4 Schematic illustrating input parameters for the TIRP methodology.

262 After evaluating a number of regression-based techniques for generating models for traffic-  
 263 induced response prediction, artificial neural networks (ANNs), which are inspired by  
 264 biological neural systems, have been selected for this study. ANNs are a powerful way of  
 265 representing nonlinear relationships between a number of input and output parameters [10]. An  
 266 ANN consists of neurons that are interconnected in various layers. Connections between the  
 267 neurons have weights that are calibrated during training to capture the actual relationship  
 268 between the input and output parameters. A key step is the selection of an appropriate  
 269 architecture of the network that maximizes its efficiency, i.e., use low computational resources  
 270 while achieving high prediction accuracy [30].

271 This study uses a multi-layer feed-forward neural network that implements the back-  
 272 propagation rule [31]. The input parameters to the ANN are locations and weights of moving  
 273 loads and the first few PC vectors computed from distributed temperature measurements. The  
 274 output parameters are response values (e.g. strains) at specific locations on the structure. The  
 275 ANN has one hidden layer and one output layer. The output layer has a single linear neuron.  
 276 The optimal number of neurons for the hidden layer is found through a trial and error approach  
 277 that gradually increases the number of neurons while evaluating the performance of the ANN  
 278 on both training and test sets. A hidden layer of 5 neurons is observed to produce consistently  
 279 good results. This is in broad agreement with previous research in SHM on the application of  
 280 ANN for data interpretation that recommend using a hidden layer composed of between 3 and  
 281 30 neurons [32,33].

### 282 2.3. Anomaly detection techniques

283 Time histories that result from subtracting the predicted thermal and traffic response from time  
 284 histories of measured response are analysed for anomalies (damage) using signal processing  
 285 techniques. The time histories are generated as follows. The differences between measured and  
 286 predicted response are referred to as prediction errors (PEs), and are computed as shown below:

287 
$$\Delta y_s = p_s - m_s \tag{Eq. 1}$$



288 where  $\Delta y_s$  is the PE, and  $p_s$  and  $m_s$  are predicted and measured response respectively at sensor  
 289  $s$ .  $m_s$  is computed as the sum of the predicted thermal response and the predicted traffic  
 290 response. The PEs computed for each time-step for a sensor are sequenced chronologically to  
 291 form a time series, which is referred to as a PE signal.

292 PE signals are expected to be stationary with a zero mean. Only changes to structural  
 293 performance due to factors unrelated to loading such as damage are expected to be left in the  
 294 signals. Such changes in signals are hard or impossible to identify without employing signal-  
 295 processing techniques. PE signals corresponding to various sensor locations can either be  
 296 analysed individually or be analysed in groups to detect anomalous structural behaviour. The  
 297 latter approach, also termed multivariate analysis, relies on the correlations between response  
 298 measured at various locations of a bridge. Damage to a bridge component will modify prior  
 299 correlations since bridges are typically well-connected structural systems such that damage  
 300 affects load paths within the structure. In previous studies, signal subtraction method (SSM)  
 301 [28] and cointegration [15] have been shown to detect anomaly events better than other signal  
 302 processing techniques such as moving principal component analysis and moving fast Fourier  
 303 transform [34]. Therefore, in this study, SSM and cointegration are employed to analyse PE  
 304 signals for anomalies.

305 **SSM** is a novel technique proposed in [28]. In SSM two PE signals are linearly combined to  
 306 generate a subtracted signal, which is then analysed for anomalies. Mathematically, it is applied  
 307 as follows:

$$308 \quad T_{kl} = \left(\frac{w_k}{f_k}\right) \Delta y_k - \left(\frac{w_l}{f_l}\right) \Delta y_l \quad (\text{Eq. 2})$$

309  $T_{kl}$  is the subtracted signal resulting from the subtraction process.  $\Delta y_k$  and  $\Delta y_l$  are values of  
 310 the PE signals corresponding to sensors  $k$  and  $l$  respectively.  $f_k$  and  $f_l$  are scaling factors for  
 311 the two PE signals. These are equal to the range of signal values in the training period, i.e., the  
 312 difference between the maximum and minimum values in the training period.  $w_k$  and  $w_l$  are  
 313 weights specified according to the accuracies of the respective sensor and its corresponding  
 314 model for thermal response prediction. In this study, the hypothesis is that measurements from  
 315 all elements are equally important. Therefore weights of all PE signals are set equal to 1.

316 **Cointegration** utilizes the statistical properties of cointegrated signals for anomaly detection.  
 317 In probability theory, a signal is said to be stationary, if its mean, variance and autocovariance  
 318 stay constant over time, and non-stationary if otherwise. A non-stationary signal is said to be  
 319 integrated to an order  $d$  if a process of taking differences over the time series repeated  $d$  times  
 320 leads to a stationary signal. In mathematical notation, the order of integration of a signal is  
 321 often denoted by  $I(d)$ . A group of signals, where each signal is  $I(1)$ , is said to be cointegrated  
 322 if there exists a linear combination of the signals that is stationary. These stationary signals are  
 323 referred to as cointegrated signals, and the process of finding them referred to as cointegration.  
 324 The concept of cointegrated signals, which was initially proposed and used in the field of  
 325 econometrics [35], was first applied to structural health monitoring by Cross et al. [15]. Cross  
 326 et al. [15] showed that it is useful for purging quasi-static effects in measurements, and

327 demonstrated its performance using measurements from a few benchmark problems including  
328 the National Physical Laboratory Footbridge in the UK [36].

329 In this paper, cointegration is applied on PE signals, which are typically non-stationary  
330 processes since the predicted structural response does not perfectly match the measured  
331 response. The premise is that the stationarity of a cointegrated signal derived from PE signals  
332 will be affected by an anomaly event. Given  $n$  PE signals,  $n - 1$  cointegrated signals can be  
333 generated. Cointegrated signals are generated and evaluated within the MATLAB environment  
334 as explained below. The full details of the mathematics behind cointegration can be found in  
335 [15].

336 Step 1 Test PE signals for stationarity. Non-stationary signals are then converted to signals  
337 that are integrated to order one. Augmented Dickey-Fuller [37] test is used to  
338 examine the stationarity of a signal. The `adftest` function provided in the  
339 MATLAB Econometrics Toolbox [38] is used for this test.

340 Step 2 Select signals which have passed the Augmented Dickey-Fuller stationarity test.

341 Step 3 Apply the Johansen cointegration procedure [39] to find suitable cointegrating  
342 vectors. In this study, the `jcitest` function in MATLAB Econometrics Toolbox  
343 [38] is used to find the cointegrating vectors.

344 Step 4 Project response measurements into the space of cointegrated vectors. These  
345 projected vectors are termed cointegrated residuals and when sequenced  
346 chronologically form cointegrated signals.

347 Both SSM and cointegration fundamentally require computing and tracking the time-evolution  
348 of a damage sensitive feature. An anomaly is said to be detected when the evaluated damage  
349 sensitive feature, which is a subtracted signal when using SSM and a cointegrated signal when  
350 using cointegration, exceeds a predefined confidence interval. Mean ( $\mu$ ) and standard deviation  
351 ( $\sigma$ ) values during the reference period are computed to derive thresholds for the confidence  
352 interval:

$$353 \quad [\mu - n\sigma, \mu + n\sigma] \quad (\text{Eq. 3})$$

354 where  $n$  is the number of standard deviations defining the range of the confidence interval.  
355 According to previous studies,  $n = 3$  and  $n = 6$  are chosen to set confidence intervals for  
356 damage sensitive features in cointegration and SSM, respectively. Both anomaly detection  
357 techniques are briefly described below giving particular attention to the damage sensitive  
358 features used in this study.

### 359 3. Case study

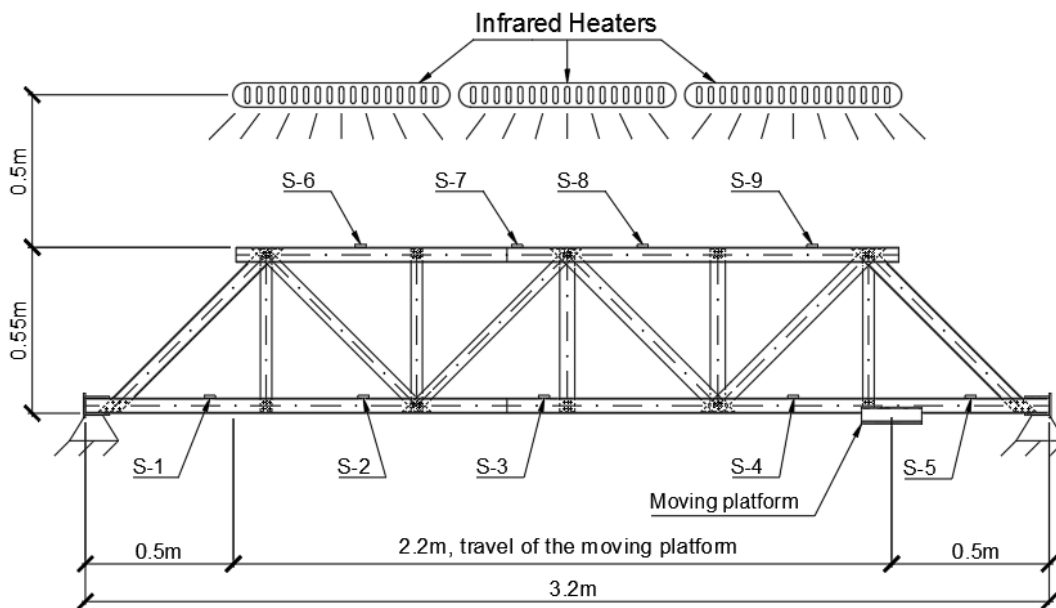
360 The performance of the measurement interpretation approach proposed in the previous section  
361 is evaluated on measurements collected from a laboratory structure: a truss that is subjected to  
362 accelerated temperature variations and periodically applied moving loads.

363 **3.1. Experimental setup**

364 A sketch of the truss depicting its principal dimensions and the location of sensors is shown in  
 365 Figure 5. Further details on the truss are available in authors' previous work [28]. Temperature  
 366 variations are simulated with three infrared heating lamps (Figure 5). They are installed 0.5 m  
 367 above and 0.2 m behind the truss. The lamps are plugged in to the mains through timer plugs  
 368 which turn them on every 1½ hours for ¾ of an hour. This set-up allows simulating 16  
 369 temperature cycles in a day. Temperatures in the truss are monitored with 31 thermocouples  
 370 and a thermal imaging camera (TIC).

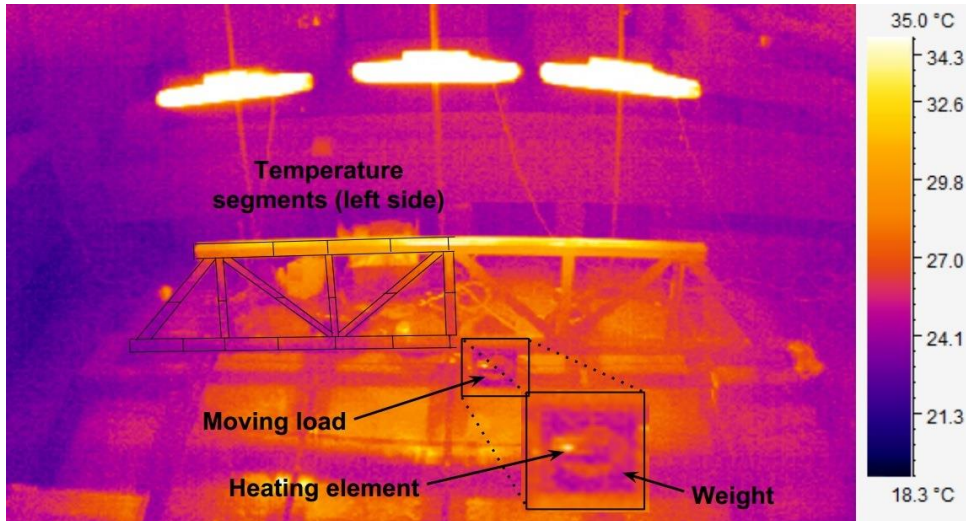
371 Moving loads are simulated using a mobile platform installed on the bottom chord of the truss  
 372 (Figure 5) that is driven by a motor. While the speed of the moving platform can be adjusted  
 373 by altering the power supply to the motor that drives it, the maximum speed at which the  
 374 platform can be pulled is still much lower than the average speeds of vehicles crossing full-  
 375 scale bridges. A heating element in the form of a one-watt power resistor is attached to the  
 376 moving platform. The location of the moving load is detected by processing thermal images,  
 377 and is defined in terms of its distance from the left support of the truss by assuming that the  
 378 total length of travel of the platform is 100 units. This concept is shown in Figure 6.

379 Weights are added onto the platform to simulate traffic loads. This study uses five different  
 380 moving load cases – 0 N, 40 N, 100 N, 140 N and 180 N, which are from hereon denoted as  
 381 L-0, L-1, L-2, L-3 and L-4 respectively. Each non-zero load case is applied for up to four  
 382 simulated diurnal cycles. The weights are altered only when the platform is at the right end of  
 383 the truss, and the motor is turned off. For case L-0 that is without traffic loading the platform  
 384 is kept stationary at the right end of the truss. The structure's response is measured at various  
 385 locations (see Figure 5) with 9 linear-pattern foil strain gauges. Response measurements are  
 386 collected at a rate of six measurements per minute.



387

388 Figure 5 A sketch of the test-bed with its principal dimensions and the location of  
 389 strain gauges (S-*i*, *i* = 1, 2, ..., 9).



390

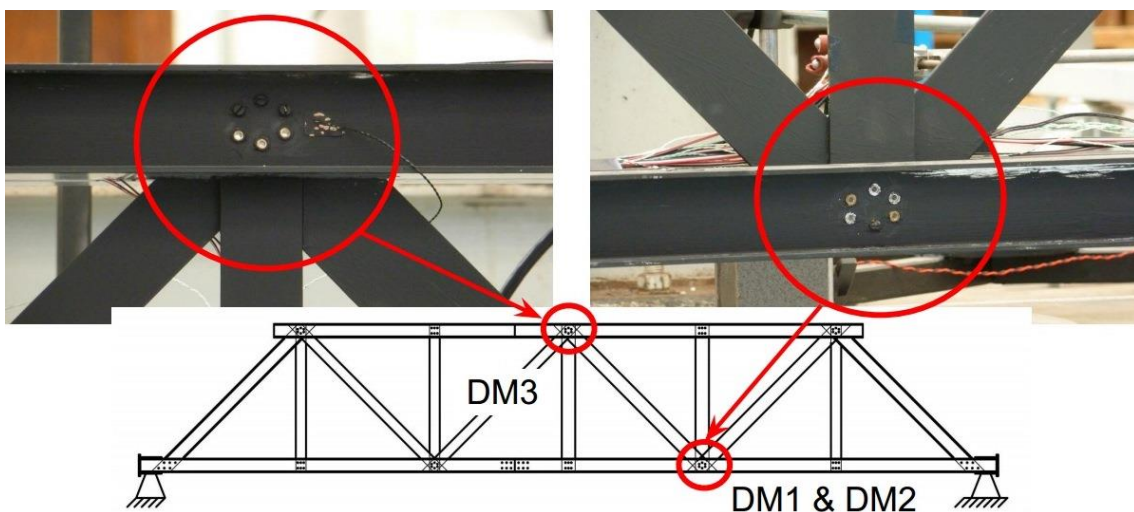
391 Figure 6 Thermal image of the experimental set-up with a close-up view of the moving  
 392 load and heating element.

393 **Damage scenarios**

394 The truss is monitored in both healthy and damaged states. Three damage scenarios, which are  
 395 referred to as DM1, DM2 and DM3, are considered. These scenarios are shown in Figure 7  
 396 and listed below:

- 397 DM1 - Three bolts are removed from the joint connecting two diagonal and one vertical  
 398 elements to the bottom chord;
- 399 DM2 - Two additional bolts are removed from the same joint named in DM1;
- 400 DM3 - Three bolts are removed from a joint on the top chord.

401 Scenarios DM1, DM2 and DM3 last for 47, 46 and 46 simulated diurnal cycles (or  
 402 approximately 25,000 measurements in total). At the end of scenario DM3, the truss is repaired  
 403 by putting back all the removed bolts; this event is denoted as scenario F.



404  
 405

Figure 7 Joints affected by simulated damage scenarios.

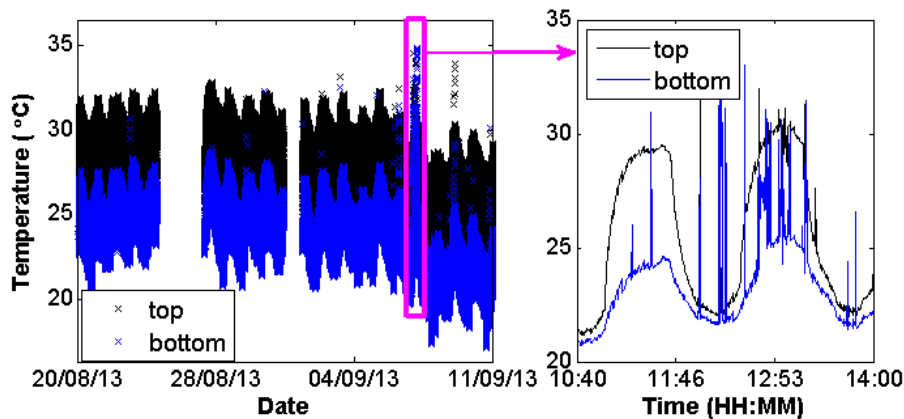
406 **3.2. Measurement time histories**

407 **Temperatures**

408 Temperature time histories are derived from thermal images collected by the TIC and the  
409 measurements from the thermocouples. Thermal images are processed as follows. The area of  
410 the truss in the thermal images is divided into segments (see Figure 6). The average temperature  
411 is calculated for each segment from each thermal image. In total, 42 segments are created as  
412 follows:

- 413 • the top and bottom chords are divided in 8 and 12 segments each, and
- 414 • each element between the top and bottom chords is split into two segments leading to  
415 22 segments in total.

416 Temperature variations computed for the top and bottom chords are shown in Figure 8 (left).  
417 The plots show that the temperature in the laboratory is affected by the outside air temperature.  
418 The temperature variations induced by the infrared heaters are superimposed on the variations  
419 in the ambient temperature. A closer look at the time histories reveals the simulated diurnal  
420 cycles (Figure 8 (right)). The time histories also show disruptions to data collection, outliers  
421 and noise, commonly seen also in measurements from full-scale structures. Disruptions were  
422 due to problems related to storing the thermal images. These disruptions are removed to have  
423 continuous measurement-histories. Outliers were generated occasionally when the field-of-  
424 view of the TIC was partially blocked such as during the presence of a human when the weights  
425 on the moving platform are modified.



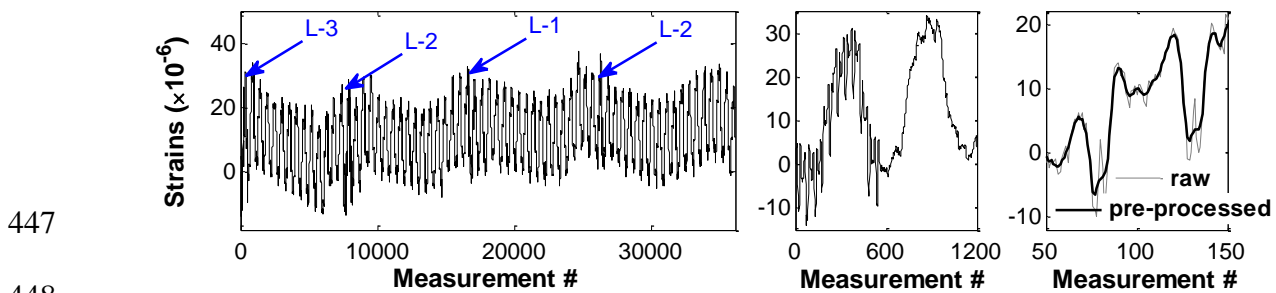
426  
427 Figure 8 Time histories of temperatures calculated from segments of the top and bottom  
428 chord (Figure 6) with those for the entire monitoring period on the left and a closer look at  
429 two simulated diurnal cycles on the right.

430 **Response**

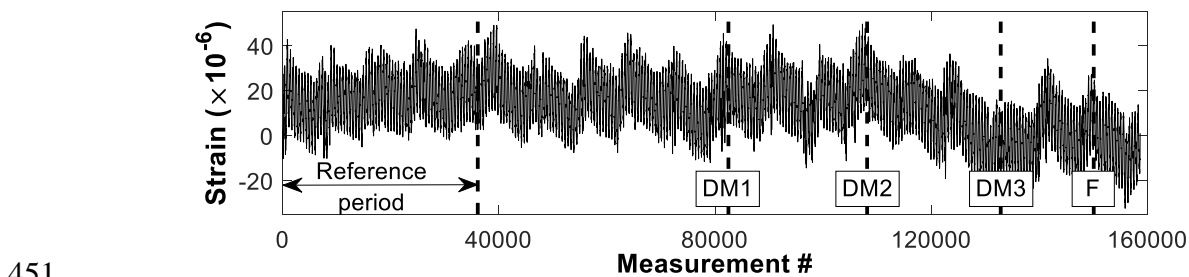
431 Response measurements have been collected with no interruptions. However, in order to keep  
432 them compatible with the temperature signals, measurements corresponding to periods when  
433 thermal images have not been recorded are omitted from response time histories. Figure 9  
434 shows plots of the measurement time histories produced by sensor S-2. The plot on the left  
435 shows the first 36,000 measurements in the time histories. The figure also includes closer views  
436 of response variations during a simulated diurnal cycle. The plots show that variations in

437 ambient temperature as well as the radiation from the infra-red lamps affect the structural  
 438 response.

439 The response due to the moving loads are seen superimposed on the response due to simulated  
 440 diurnal cycles in the form of a noisy pattern (Figure 9 (middle)). Strains spike when the moving  
 441 platform passes by the sensor location S-2 (see Figure 9 (right), between measurements #100  
 442 and #150). The complete strain signals produced by sensors S-4, which are located close to the  
 443 joint involved in damage scenarios DM1 and DM2, are shown in Figure 10. Strain  
 444 measurements closely resemble variations in temperatures (Figure 10). While a gradual drift  
 445 of the signal is observed after damage event DM2, at this time the ambient temperature has  
 446 also decayed (see Figure 8 around 7/11/2013).

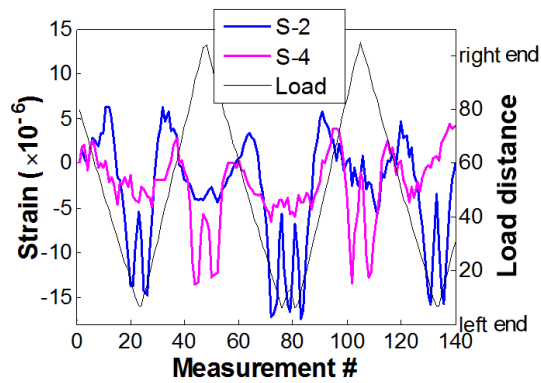


449 Figure 9 Strains measured with sensor S-2 (right) and closer views (middle and left) of  
 450 the time histories to understand the effects of moving load.



451 Figure 10 Strain signals as measured with S-4; also shown are the time of initiation of  
 452 the various damage scenarios.  
 453

454 Figure 11 shows strain signals in relation to the location of the moving load as computed from  
 455 the thermal images. The correlations between the strains and locations of the moving load are  
 456 such that the location of the moving load can even be defined accurately from the measured  
 457 response.



458

459

460

Figure 11 Locations of the moving load computed from thermal images plotted alongside strains.

461

## 4. Results

462

463

464

465

466

467

In this section, the proposed measurement interpretation approach is evaluated on measurements collected from the laboratory truss. The RBTRP methodology and then the TIRP methodology are employed to generate statistical models for predicting temperature-induced and traffic-induced response respectively. The PE signals, which are derived after purging the effects of temperature and traffic loads from measurement time histories, are then processed using anomaly detection techniques.

468

### 4.1. Response predictions

469

#### Reference period

470

471

472

473

474

475

476

477

Measurements from the first 66 simulated diurnal cycles (see Figure 10) form the reference period for evaluating the proposed approach. Measurements taken during this period are plotted in Figure 9 (left). Periods when the moving load is present, are excluded from the reference data-set for the RBTRP methodology. The four periods when the moving load is present in the reference period as indicated in Figure 9 (left) form the reference-data set for the TIRP methodology. Load L-4 has not been deployed during the reference period. This study will examine if the response due to L-4 can be predicted accurately using regression models that are generated based solely on the loads present during the reference period.

478

#### Thermal response prediction

479

480

481

482

The RBTRP methodology is employed to derive regression models to predict thermal response. Regression models are generated using temperatures collected using the TIC. High prediction accuracies, as evaluated in terms of root mean square error (RMSE), are obtained for strain predictions when:

483

484

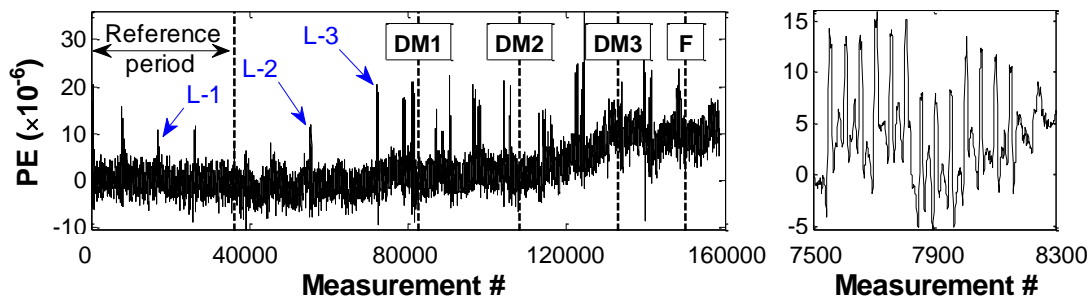
485

486

- the input temperature measurements are down-sampled to  $1.2 \times 10^{-2}$  Hz,
- the number of PCs is set to 14, and
- the PCs corresponding to the current time-step and the previous time-step are provided as input to the regression models for accounting for thermal inertia effects.



487 A PE signal computed for sensor location S-2 is plotted in Figure 12. A PE signal for a specific  
 488 sensor is denoted as PE *sensor name*, for example, PE S-2 refers to a PE signal for sensor  
 489 location S-2. If noise in thermal response predictions and measurement noise follow a Gaussian  
 490 distribution, the PE signals will resemble a stationary signal. A deviation from stationarity such  
 491 as in the form of a change to the mean of the signal may indicate the presence of the moving  
 492 load. Spikes due to the moving loads are discernible in PE S-2 shown in Figure 12. A closer  
 493 examination of PE S-2 during the period when load L-2 is applied reveals that thermal effects  
 494 have not been fully removed from response measurements (Figure 12 (right)). PE values at the  
 495 sensor location S-2 rise abruptly from 0 to  $15 \times 10^{-6}$  when the moving load is applied (near  
 496 measurement #7510). With respect to damage scenarios, a gradual shift in the mean of PE S-2  
 497 can be noticed shortly after scenario DM2. However, other scenarios are not detectable from  
 498 the PE signals.



499  
500

501 Figure 12 The variation of PEs for sensor location S-2 is plotted to show the effect of the  
 502 moving load and temperature (left), and a closer view of the signal (right).

503 Next, regression models are generated using temperature measurements from thermocouples  
 504 in order to compare its performance with those generated using measurements from the TIC.  
 505 As when using data from the TIC, temperature measurements are down-sampled to  $1.2 \times 10^{-2}$   
 506 Hz. 10 PCs are required to capture 99.99% of the variability in temperature measurements.

507 Table 1 presents data on the accuracy of the regression models produced for thermal response  
 508 prediction using temperature data from thermocouples and the TIC. The accuracy is expressed  
 509 using a parameter  $e_p$ , which is a measure of error computed in terms of the range of measured  
 510 strains for a group of sensors (see Eq. 4).

$$511 \quad e_p = \frac{1}{n} \sum_{s=1}^n \frac{e_s}{r_s} \quad (\text{Eq. 4})$$

512  $n$  is the number of sensors;  $e_s$  is the root mean squared error in predictions and  $r_s$  is the range  
 513 of measured strains at sensor  $s$ . The sensors on the top and bottom chords are analysed  
 514 separately in two groups. The mean range of the measured strains is:

- 515 •  $68 \times 10^{-6}$  strains collected with five strain sensors on the bottom chord;
- 516 •  $138 \times 10^{-6}$  strains collected with four strain sensors on the top chords;

517 Results in Table 1 show that regression models generated using temperature measurements  
 518 collected by both TIC and thermocouples demonstrate high accuracy.



519 Table 1: Accuracy (expressed in terms of  $e_p$ ) of the regression models generated using  
 520 temperature measurements from thermocouples (noted as TH in the table) and the TIC.

	Bottom chord (strains)		Top chord (strains)	
	TH	TIC	TH	TIC
$e_p$ (%)	4.2%	3.7%	1.8%	1.8%

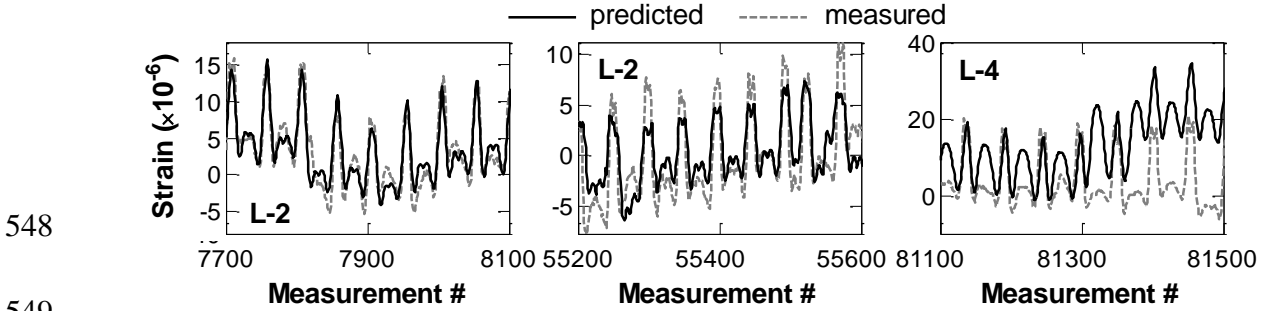
521 **Traffic-induced response predictions**

522 The PE signals computed using measurements from the TIC are next treated for effects of the  
 523 moving loads. The results presented in Figure 12 (right) show that temperature effects are still  
 524 present even after subtracting predicted thermal response from the measured response. This is  
 525 evident from the underlying sinusoidal variation in the trend, which corresponds directly to the  
 526 simulated diurnal cycle. For this reason, predicting the vehicular response requires information  
 527 regarding temperatures. Hence information of the magnitude of the applied load and its location  
 528 and the first few PCs of temperatures are selected as input variables for the TIRP methodology.  
 529 Combinations of the measurement input frequency and number of PCs are evaluated. The best  
 530 results are found when the input traffic measurements are down-sampled to  $5 \times 10^{-2}$  Hz and the  
 531 number of PCs is set to 4.

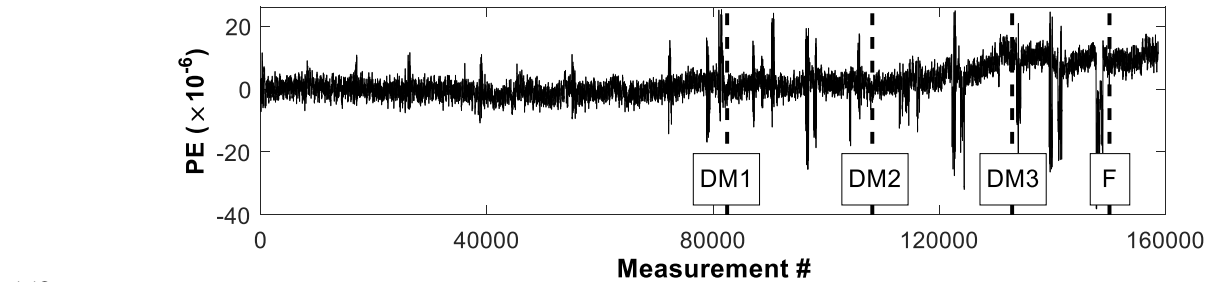
532 The predicted and measured traffic-induced response for three periods over the monitored  
 533 duration are provided in Figure 13. These periods are described below:

- 534 • Period A, which is within the reference period, and comprises measurements #7,000 to  
 535 #8,100 during which load L-2 is applied (Figure 13 (left));
- 536 • Period B, which is outside the reference period but before the introduction of damage  
 537 scenarios, and comprises measurements #55,200 to #55,600 during which load L-2 is  
 538 applied (Figure 13 (middle)), and
- 539 • Period C, which is outside the reference period but before the introduction of damage  
 540 scenarios, and comprises measurements #81,100 to #81,500 during which load L-4, a  
 541 moving load unexperienced during the reference period, is applied (Figure 13 (right)).

542 Predicted and measured strains are in good agreement for periods A and B. However, the  
 543 discrepancy in predictions is comparatively large for the period C (Figure 13 (top)) when L-4  
 544 was applied. Response due to L-4 cannot be predicted accurately using regression models that  
 545 are generated based solely on the loads present during the reference period. Hence, all types of  
 546 loads have to be included in the regression model generation. A plot of PE S-2 is provided in  
 547 Figure 14.



550 Figure 13 Measured and predicted strains during period A (left), period B (middle) and  
551 period C (right).



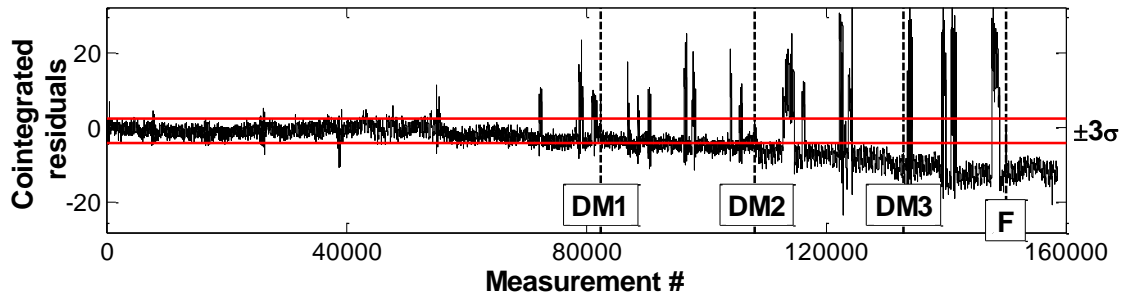
553 Figure 14 PE signals derived after subtracting traffic-induced and thermal response from  
554 measurements collected by sensor S-2.

555 **4.2. Anomaly detection**

556 In this section, anomaly detection techniques are employed to interpret the time histories of  
557 data. First, anomaly detection techniques are used on prediction error signals computed by  
558 subtracting both predicted thermal and traffic response from measured response. Next, to  
559 understand the effectiveness of subtracting traffic response from the measurements, anomaly  
560 detection techniques are used on the error signals computed by subtracting only predicted  
561 thermal response from measured response. Then, anomaly detection techniques are employed  
562 directly on the time histories of response measurements to demonstrate the importance of  
563 having models to predict thermal and traffic-induced response.

564 **Interpretation of prediction error (PE) signals**

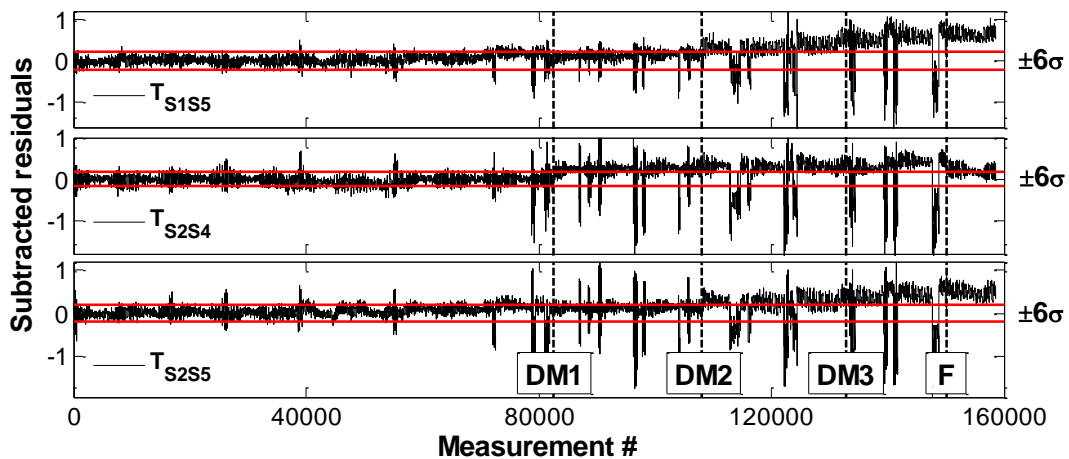
565 Cointegration: The PE signals derived in Section 4.1 are first analysed for anomaly events with  
566 the cointegration technique. The first  $\frac{1}{3}$ <sup>rd</sup> of measurements from the reference period forms the  
567 data-set used to derive the cointegration model. The confidence interval is defined using values  
568 of cointegrated residuals from the reference period. The computed cointegrated signal is plotted  
569 in Figure 15. Spikes and temporary shifts in the signal are indicative of periods when moving  
570 loads are present. The larger spikes before DM1 represent periods when L-4 is applied. Values  
571 of cointegrated residuals are observed to deviate away from the confidence interval as the  
572 damage severity increases. The trend departs gradually from the confidence interval after DM1  
573 and it permanently departs the confidence interval after DM2.



574

575 Figure 15 Cointegrated residuals of signals computed in Section 4.2.

576 SSM: Two PE signals are combined to create one SSM signal. For example, subtracted signal  
 577  $T_{S1S5}$  is a combination of PE signals from sensor location S-1 and S-2. For DM1 and DM2, the  
 578 joint that lies between sensor locations S-3 and S-4 is damaged. The subtracted signals created  
 579 from the signals corresponding to the two sensor locations are expected to reflect anomaly  
 580 events. However, all combinations of PE signals from strain sensors located on the bottom  
 581 chord show evidence of anomaly events, and especially subtracted signals created from those  
 582 signals corresponding to sensors S-1 and S-2. Figure 16 plots three subtracted signals –  $T_{S1S5}$ ,  
 583  $T_{S2S4}$  and  $T_{S2S5}$ , all of which indicate anomaly events. Similar to cointegrated signals, periods  
 584 when the moving loads are present can be seen as spikes in values of subtracted residuals.  $T_{S1S5}$   
 585 and  $T_{S2S5}$  permanently exceed the confidence interval after DM2.  $T_{S2S4}$  departs from the  
 586 confidence interval soon after DM1.  $T_{S2S4}$  deviates further from the upper bound of the  
 587 confidence interval with increasing damage severity. When the structure is mended at event F,  
 588 the signal tends to return to the confidence interval. The values of subtracted residuals of other  
 589 signals hold steady after the truss is repaired during event F.



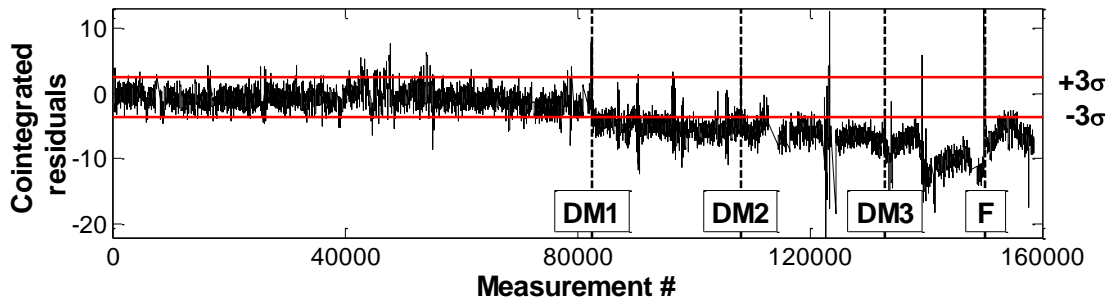
590

591 Figure 16 SSM residuals  $T_{S1S5}$ ,  $T_{S2S4}$  and  $T_{S2S5}$  for signals computed in Section 4.1.

592 **Interpretation of signals without thermal response**

593 In order to assess the impact of moving loads on anomaly detection, measurements taken  
 594 without having moving loads on the structure are now analysed separately. PE signals derived  
 595 from subtraction of the thermal response from these measurements are analysed using anomaly  
 596 detection techniques. When the periods of moving loads are excluded from the measurement  
 597 interpretation, signal trends become much less noisy. As an example, a cointegrated signal is

598 generated and plotted in Figure 17. The cointegrated signal has a few spikes and has no shifts  
 599 when compared to the cointegrated signal plotted in Figure 15. Shifts in the signal due to  
 600 anomaly events are distinguishable, especially those due to anomaly events DM1, DM3 and F.  
 601 Similar results are achieved when interpreting the same data-set with SSM. They are not plotted  
 602 here for reasons of brevity.

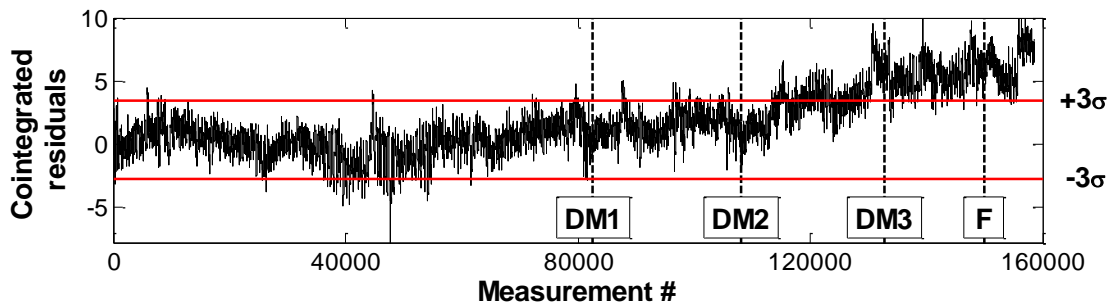


603

604 Figure 17 Cointegrated residuals generated from PE signals for measurement periods  
 605 when no moving load is present.

606 **Interpretation of response measurements**

607 A plot of a cointegrated signal generated using collected strain measurements is provided in  
 608 Figure 18. The signal starts to drift gradually from the confidence interval shortly after DM2,  
 609 and the signal permanently departs the confidence interval after DM3. Figure 15 and Figure 17  
 610 show that anomaly events can be detected sooner by analysing the signals generated after  
 611 subtracting traffic-induced and thermal response than by direct analysis of response  
 612 measurements. This conclusion of faster and more reliable damage detection using PE signals  
 613 has already been confirmed [34].



614

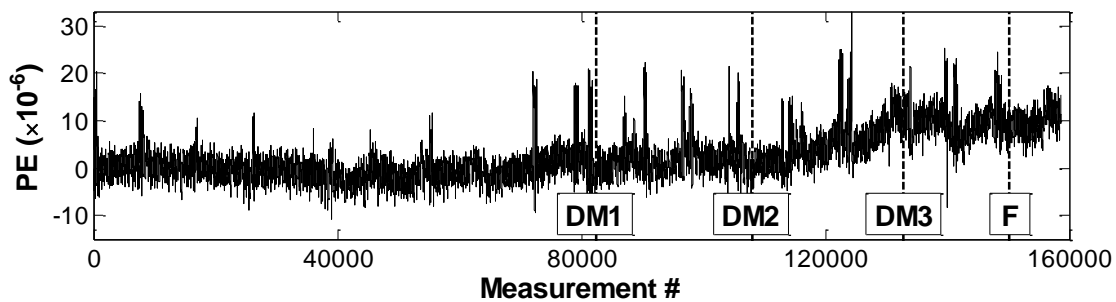
615 Figure 18 Cointegrated residuals of strain measurements.

616 **4.3. Application of the temperature-based measurement interpretation**  
 617 **approach**

618 This study lastly evaluates the application of the temperature-based measurement interpretation  
 619 approach proposed in [28]. The idea here is to evaluate if thermal effects alone can form the  
 620 basis of measurement interpretation without giving consideration to the presence or absence of  
 621 moving loads on the structure. Comparing results from this approach with those presented in  
 622 Sections 4.1 and 4.2 using TIRP methodology will enable us to ascertain if knowledge of traffic  
 623 loads helps with measurement interpretation.

624 The temperature-based measurement interpretation approach is similar to the measurement  
 625 interpretation approach presented in Section 2 but with two key differences. First, it does not  
 626 include the TIRP methodology. Second, training of the regression models in RBTRP  
 627 methodology is done using all available data during the reference period including response  
 628 data collected when moving loads are present.

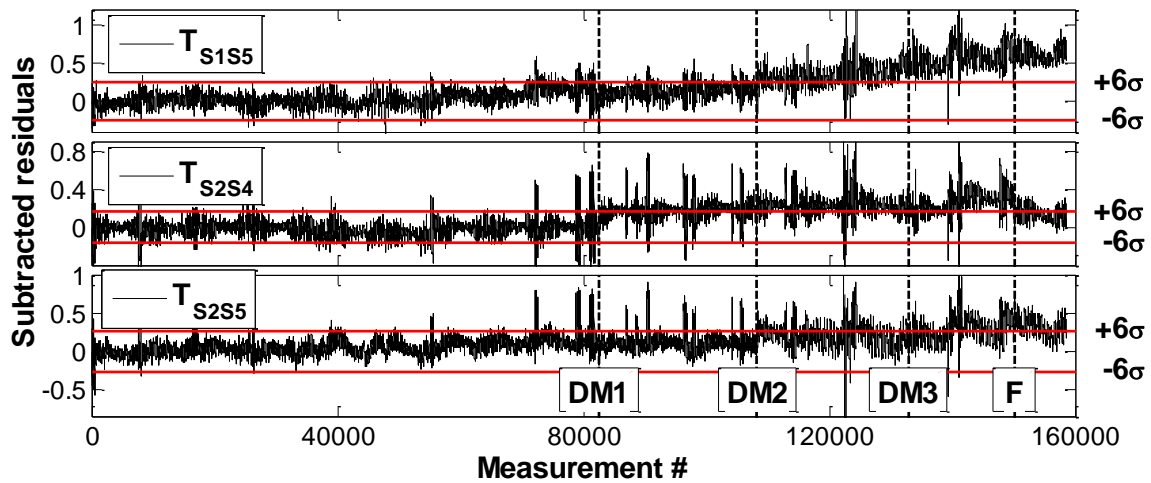
629 Response predictions: The reference period used for the regression model generation of thermal  
 630 response prediction is the same as used in Section 4.1, i.e. 66 simulated diurnal cycles.  
 631 However the measurement time histories are not separated into two data sets according to  
 632 whether they have moving loads or not as described in Section 2. A data-set that comprises all  
 633 strain measurements including those that have effects of moving loads during the reference  
 634 period is selected as input to the RBTRP methodology. The  $e_p$  (see Eq. 4) values for predictions  
 635 is 3.2%. These are similar to the error values obtained when the RBTRP methodology is  
 636 coupled with the TIRP methodology (see Table 1). PE S-2 is plotted in Figure 19, which is  
 637 similar to the signal shown in Figure 12. PE values spike for periods when moving loads are  
 638 present.



639

640 Figure 19 PE S-2 derived from unfiltered strain measurements.

641 Anomaly detection: PE signals are inspected for anomaly events using the same parameter  
 642 settings as used in Section 4.2. Both SSM and cointegration show reasonably good and  
 643 comparable results. For reasons of brevity, signals generated using SSM only are discussed.  
 644  $T_{S1S5}$ ,  $T_{S2S4}$  and  $T_{S2S5}$  (similar to those shown in Figure 16) are plotted in Figure 20. Drifts in  
 645 subtracted signals are not as emphasized as in the signals plotted in Figure 16. The onset  
 646 of damage can be recognized only in  $T_{S1S5}$  (Figure 20) when the signal permanently departs  
 647 the confidence interval. The other signals are weak indicators of anomaly events. The other  
 648 signals are weak indicators of anomaly events.



649

650 Figure 20  $T_{S1S5}$ ,  $T_{S2S4}$  and  $T_{S2S5}$  generated using SSM from PE signals (see Section 0)

651 **4.4. Discussion**

652 This study demonstrates a new contact-free approach of measuring temperatures using a  
 653 thermal imaging camera (TIC) in the context of continuous bridge monitoring. Results show  
 654 that thermal response can be predicted accurately from the temperature distributions measured  
 655 by either a TIC or thermocouples (see Figure 6 and Figure 8). These results are validation of  
 656 the performance of the RBTRP methodology, also demonstrated previously by the authors in  
 657 [22].

658 The selection of reference period is observed to be a key factor in the performance of the TIRP  
 659 methodology. The regression models failed to predict the traffic response for load case L-4  
 660 when measurements corresponding to this loading scenario were not included in the training  
 661 data set (see Figure 13). In real-life, this would imply that the regression models would not  
 662 perform suitably for abnormal loading scenarios, which may be absent or appear rarely in the  
 663 reference data set. However, for loading scenarios that are present in the training set, the  
 664 regression models predict the traffic response with sufficient accuracy.

665 Results from the application of anomaly detection techniques on prediction error (PE) signals  
 666 and other signals computed without removing the traffic response offer interesting insights.  
 667 Both SSM and cointegration are capable of detecting some anomaly events from PE signals.  
 668 Cointegrated signals and subtracted signals show shifts after damage scenario DM-1 but these  
 669 are not significant enough (i.e. do not exceed threshold bounds) to confirm an anomaly event.  
 670 However, incremental damage through DM-2 does eventually take the signals outside the  
 671 threshold bounds (Figure 15 and Figure 16). If the threshold bounds were calibrated after  
 672 DM-2, the cointegrated signal may have also detected DM-3. None of the signals return to their  
 673 original position after scenario F when the truss is repaired. This may indicate that the  
 674 connection stiffnesses of the joints, where bolts were removed, were permanently altered and  
 675 were not taken back to their original states when the same bolts were re-inserted. The anomaly  
 676 detection techniques perform better when applied on the portion of the measurements that are  
 677 without traffic response (see Figure 17). This indicates that, on bridges where there are periods  
 678 with minimal vehicle loading, the proposed approach can be adapted to analyse measurements

679 that contain only thermal response. A lot of short- and medium-span bridges in the road  
680 network have significantly less traffic during night times and may fall in this category.

681 Anomaly detection techniques show better performance when applied on PE signals than when  
682 applied directly on response time series. This indicates that subtracting thermal response and  
683 vehicle response from response measurements improves the chances of anomaly detection. The  
684 particular importance of subtracting vehicle response is confirmed by the last set of results on  
685 the performance of the temperature-based measurement interpretation approach that ignores  
686 the presence or absence of traffic loads while accounting for thermal response. These results  
687 support the idea of devising measurement interpretation techniques that focus on explicitly  
688 accounting for the effect of various loads (e.g. traffic, temporary works) and environmental  
689 parameters (e.g. temperature, wind) to support reliable detection of anomaly events. Lastly, it  
690 must be noted that anomaly detection techniques are meant to support engineers in decision-  
691 making. Engineering judgment and knowledge will be required to decide on the course of  
692 action upon notification of an anomaly event. Actions could be in the form of on-site  
693 inspections and augmentation of the monitoring system.

#### 694 **4.5. Limitations**

695 The focus of this study is on the interpretation of measurements rather than measurement  
696 collection, which can itself be a challenging task. For instance, most highway bridges have  
697 continuous traffic flow on multiple lanes and will require sophisticated vision-based  
698 monitoring systems to capture data on the traffic and its loads. The collection of images and  
699 their subsequent processing to produce data on the locations and weights of the vehicles is a  
700 computational challenge that is solvable [40].

701 The case study used in this study is a laboratory setup of a much smaller scale than a real-life  
702 structure. In a full-scale bridge, strain measurements have dynamic effects that are determined  
703 by the weight and the speed of the vehicle and the profile of the road surface in addition to the  
704 bridge structural characteristics (e.g. natural frequency). Also, only one vehicle was considered  
705 to be on the laboratory structure at any given time, an aspect which is not true in real-life  
706 bridges. A natural next step is therefore to test and evaluate the proposed approach using  
707 measurements from potentially a short-span full-scale bridge.

#### 708 **5. Conclusions**

709 A novel measurement interpretation approach to predict traffic-induced and thermal response  
710 of bridges using measurements of distributed temperature and traffic loads and their locations  
711 is proposed in this paper. This approach is investigated using measurements from a laboratory  
712 structure that is exposed to accelerated temperature variations. Traffic loads are simulated using  
713 a moving platform that travels along the bottom chord of the truss and can hold adjustable  
714 weights. Response measurements are collected with contact sensors (e.g. strain gauges), and  
715 temperature distributions are captured with a thermal imaging camera and thermocouples. The  
716 structure is monitored in health and damaged states. Traffic-induced and thermal response are  
717 predicted and subsequently removed from the measured response time histories. In the process,

718 prediction error signals are created. These signals are then interpreted with anomaly detection  
719 techniques.

720 This experimental study draws the following conclusions:

- 721 • Thermal images can be used to measure temperature distributions at accuracies  
722 sufficient for data interpretation. Both regression models generated with temperature  
723 measurements from the thermal imaging camera and from the thermocouples show high  
724 prediction accuracies.
- 725 • When moving loads are present, thermal effects are not removed completely from  
726 response measurements by predicted thermal response. For this reason, in addition to  
727 information of the magnitude of the applied load and its location, the first few PCs of  
728 temperatures are also needed as input variables for the TIRP methodology.
- 729 • All types of traffic loads have to be included in the reference period to create robust  
730 statistical models for traffic-induced response prediction. If certain load cases are  
731 excluded, then TIRP fails to accurately predict traffic response for those scenarios.
- 732 • The proposed TIRP methodology is unable to fully eliminate the effect of moving loads  
733 on measured response. Consequently anomaly detection is observed to be better when  
734 measurements collected during traffic loads are excluded from the data set.

735 The proposed integrated approach needs further development to integrate a broader range of  
736 traffic scenarios and validation on measurements from real-life structures with high thermal  
737 mass. The TIRP methodology, which aims to predict traffic-induced response, needs further  
738 integration with sensing technologies for applications to full-scale structures. TICs need to be  
739 employed continuously on full-scale bridges to certify their scalability. In the experimental  
740 setup, the laboratory truss was coated with a matt black paint hence reduction surface reflection  
741 which might be an issue when monitoring full-scale bridges.

## 742 6. References

- 743 [1] J. Brownjohn, Structural health monitoring of civil infrastructure, *Philos Trans. A Math*  
744 *Phys Eng Sci.* 365 (2007) 589–622.
- 745 [2] R.S. Adhikari, O. Moselhi, A. Bagchi, Image-based retrieval of concrete crack  
746 properties for bridge inspection, *Autom. Constr.* 39 (2014) 180–194.  
747 doi:10.1016/j.autcon.2013.06.011.
- 748 [3] Roads Liaison Group, *Management of Highway Structures - A Code of Practice*, 2013.
- 749 [4] UK Transport Committee, *Memorandum from UK Roads Liaison Group*, 2010.  
750 [http://www.publications.parliament.uk/pa/cm200910/cmselect/cmtran/473/473we04.ht](http://www.publications.parliament.uk/pa/cm200910/cmselect/cmtran/473/473we04.htm)  
751 [m](http://www.publications.parliament.uk/pa/cm200910/cmselect/cmtran/473/473we04.htm).
- 752 [5] FHWA, *Tables of Frequently Requested NBI Information*, (2015).  
753 <https://www.fhwa.dot.gov/bridge/britab.cfm> (accessed August 30, 2016).
- 754 [6] E.J. Cross, K.Y. Koo, J.M.W. Brownjohn, K. Worden, Long-term monitoring and data  
755 analysis of the Tamar Bridge, *Mech. Syst. Signal Process.* 35 (2013) 16–34.  
756 doi:<http://dx.doi.org/10.1016/j.ymsp.2012.08.026>.
- 757 [7] H. Sousa, C. Félix, J. Bento, J. Figueiras, Design and implementation of a monitoring



- 758 system applied to a long-span prestressed concrete bridge, *Struct. Concr.* 12 (2011) 82–  
759 93.
- 760 [8] R. Kromanis, P. Kripakaran, B. Harvey, Long-term structural health monitoring of the  
761 Cleddau bridge: evaluation of quasi-static temperature effects on bearing movements,  
762 *Struct. Infrastruct. Eng.* 2479 (2015) 1–14. doi:10.1080/15732479.2015.1117113.
- 763 [9] D. Inaudi, B. Glisic, Continuous monitoring of concrete bridges during construction and  
764 service as a tool for data-driven bridge health monitoring, in: *Adv. Bridg. Maintenance,*  
765 *Saf. Manag. Life-Cycle Performance, Proc. Third Int. Conf. Bridg. Maintenance, Saf.*  
766 *Manag.*, 2006: pp. 421–422. <http://www.scopus.com/inward/record.url?eid=2-s2.0-56749155028&partnerID=40&md5=64976977b5ee0174d52531ca750d06e1>.  
767
- 768 [10] H. Sohn, K. Worden, C. Farrar, Statistical Damage Classification under Changing  
769 Environmental and Operational Conditions, *J. Intell. Mater. Syst. Struct.* 13 (2002).
- 770 [11] F.N. Catbas, M. Susoy, D.M. Frangopol, Structural health monitoring and reliability  
771 estimation: Long span truss bridge application with environmental monitoring data, *Eng.*  
772 *Struct.* 30 (2008) 2347–2359.
- 773 [12] N. Hoult, P. Fidler, Long-term wireless structural health monitoring of the Ferriby Road  
774 Bridge, *J. Bridg. Eng.* 15 (2010) 153–159.  
775 [http://ascelibrary.org/doi/abs/10.1061/\(ASCE\)BE.1943-5592.0000049](http://ascelibrary.org/doi/abs/10.1061/(ASCE)BE.1943-5592.0000049) (accessed April  
776 5, 2014).
- 777 [13] B. Peeters, G. De Roeck, One-year monitoring of the Z 24-Bridge: environmental effects  
778 versus damage events, *Earthq. Eng. Struct. Dyn.* 30 (2001) 149–171.
- 779 [14] K. Worden, C.R. Farrar, G. Manson, G. Park, The fundamental axioms of structural  
780 health monitoring, *Proc. R. Soc. A Math. Phys. Eng. Sci.* 463 (2007) 1639–1664.
- 781 [15] E.J. Cross, K. Worden, Q. Chen, Cointegration: a novel approach for the removal of  
782 environmental trends in structural health monitoring data, *Proc. R. Soc. A Math. Phys.*  
783 *Eng. Sci.* 467 (2011) 2712–2732. doi:10.1098/rspa.2011.0023.
- 784 [16] D. Posenato, P. Kripakaran, D. Inaudi, I.F.C. Smith, Methodologies for model-free data  
785 interpretation of civil engineering structures, *Comput. Struct.* 88 (2010) 467–482.
- 786 [17] Y.-L. Ding, G.-X. Wang, P. Sun, L.-Y. Wu, Q. Yue, Long-Term Structural Health  
787 Monitoring System for a High-Speed Railway Bridge Structure, *Sci. World J.* 2015  
788 (2015) 1–17. doi:10.1155/2015/250562.
- 789 [18] E. Figueiredo, E. Cross, Linear approaches to modeling nonlinearities in long-term  
790 monitoring of bridges, *J. Civ. Struct. Heal. Monit.* 3 (2013) 187–194.  
791 doi:10.1007/s13349-013-0038-3.
- 792 [19] R. Kromanis, P. Kripakaran, Support vector regression for anomaly detection from  
793 measurement histories, *Adv. Eng. Informatics.* 27 (2013) 486–495.
- 794 [20] I. Laory, T.N. Trinh, I.F.C. Smith, Evaluating two model-free data interpretation  
795 methods for measurements that are influenced by temperature, *Adv. Eng. Informatics.*  
796 25 (2011) 495–506.
- 797 [21] I. Laory, T.N. Trinh, D. Posenato, I.F.C. Smith, Combined Model-Free Data-  
798 Interpretation Methodologies for Damage Detection during Continuous Monitoring of  
799 Structures, *J. Comput. Civ. Eng.* 27 (2013) 657–666. doi:10.1061/(ASCE)CP.1943-  
800 5487.0000289.
- 801 [22] R. Kromanis, P. Kripakaran, Predicting thermal response of bridges using regression  
802 models derived from measurement histories, *Comput. Struct.* 136 (2014) 64–77.

- 803 [23] M.T. Yarnold, F.L. Moon, A.E. Aktan, Temperature-Based Structural Identification of  
804 Long-Span Bridges, *J. Struct. Eng.* (2015) 1–10. doi:10.1061/(ASCE)ST.1943-  
805 541X.0001270.
- 806 [24] B. Glisic, M.T. Yarnold, F.L. Moon, A.E. Aktan, Advanced Visualization and  
807 Accessibility to Heterogeneous Monitoring Data, *Comput. Civ. Infrastruct. Eng.* 29  
808 (2014) 382–398. doi:10.1111/mice.12060.
- 809 [25] R. Zaurin, F. Necati Catbas, Structural health monitoring using video stream, influence  
810 lines, and statistical analysis, *Struct. Heal. Monit.* 10 (2010) 309–332.  
811 doi:10.1177/1475921710373290.
- 812 [26] L.E.Y. Mimbela, L.A. Klein, Summary of vehicle detection and surveillance  
813 technologies used in intelligent transportation systems, 2000.
- 814 [27] I.T. Jolliffe, *Principal Component Analysis*, Springer-Verlag New York Inc., 2002.
- 815 [28] R. Kromanis, P. Kripakaran, SHM of Bridges: Characterising Thermal Response and  
816 Detecting Anomaly Events Using a Temperature-Based Measurement Interpretation  
817 Approach, *J. Civ. Struct. Heal. Monit.* 6 (2016) 237–254. doi:10.1007/s13349-016-  
818 0161-z.
- 819 [29] X.G. Hua, Y.Q. Ni, J.M. Ko, K.Y. Wong, Modeling of Temperature–Frequency  
820 Correlation Using Combined Principal Component Analysis and Support Vector  
821 Regression Technique, *J. Comput. Civ. Eng.* 21 (2007) 122–135.
- 822 [30] U. Dackermann, *Vibration-based damage identification methods for civil engineering  
823 structures using artificial neural networks*, University of Technology Sydney, 2010.
- 824 [31] M. Riedmiller, A Direct Adaptive Method for Faster Backpropagation Learning : The  
825 RPROP Algorithm, in: *Neural Networks, 1993., IEEE Int. Conf., IEEE, 1993: pp. 586–  
826 591.*
- 827 [32] J. Mata, Interpretation of concrete dam behaviour with artificial neural network and  
828 multiple linear regression models, *Eng. Struct.* 33 (2011) 903–910.
- 829 [33] C.E. Katsikeros, G.N. Labeas, Development and validation of a strain-based Structural  
830 Health Monitoring system, *Mech. Syst. Signal Process.* 23 (2009) 372–383.
- 831 [34] R. Kromanis, *Structural Performance Evaluation of Bridges : Characterizing and  
832 Integrating Thermal Response*, University of Exeter, 2015.
- 833 [35] J.H. Stock, M.W. Watson, Testing for common trends, *J. Am. Stat. Assoc.* 83 (1988)  
834 1097–1107.
- 835 [36] K. Worden, E. Cross, E. Barton, Damage detection on the NPL Footbridge under  
836 changing environmental conditions, in: *6th Eur. Work. Struct. Heal. Monit., Dresde,  
837 Germany, 2012: pp. 1–8.*
- 838 [37] D.A. Dickey, W.A. Fuller, Distribution of the Estimators for Autoregressive Time Series  
839 With a Unit Root, *J. Am. Stat. Assoc.* 74 (1979) 427–431. doi:10.2307/2286348.
- 840 [38] MATLAB, *Statistics Toolbox Release 2016b*, (2016).
- 841 [39] S. Johansen, Statistical analysis of cointegration vectors, *J. Econ. Dyn. Control.* 12  
842 (1988) 231–254.
- 843 [40] R. Zaurin, F.N. Catbas, Integration of computer imaging and sensor data for structural  
844 health monitoring of bridges, *Smart Mater. Struct.* 19 (2010) 15019. doi:10.1088/0964-  
845 1726/19/1/015019.
- 846